## PAPER

Check for updates

# Quantitative detection of $H_2S$ and $CS_2$ mixed gases based on UV absorption spectrometry

Xiaoxing Zhang, [iD] *[a] Zhaolun Cui,[a] Zheng Cheng,[b] Yalong Li[a] and Hai Xiao[c]

$H_2S$ and $CS_2$ are the decomposition components of insulating gas $SF_6$. The detection of these two gases is significant for the online monitoring and fault diagnosis of $SF_6$ electrical equipment. In this study, an ultraviolet (UV) differential optical absorption spectrometry (UV-DOAS) platform is established for detecting the concentration of $H_2S$ and $CS_2$ mixed gases. Based on the platform, we obtained the UV absorption spectra of the two gases. The linear relationship between each gas absorption spectra and the concentration was established by wavelet processing and frequency analysis. The interference between the two gases in the UV spectrum region was studied. $H_2S$ at different concentrations had little effect on the UV absorption spectra of $CS_2$. The linearity ($R^2$) of $CS_2$ inversion formula was 0.9997. $CS_2$ above 50 ppb produces a great interference on $H_2S$ concentration detection. $CS_2$ concentration has a linear relationship with the $H_2S$ concentration inversion; hence, the $H_2S$ correction formula with $CS_2$ concentration as the variable is proposed. With the correction formula, the linearity ($R^2$) of $H_2S$ inversion formula reaches 0.9994 in mixed gas detection, which can meet the $H_2S$ and $CS_2$ mixed gases quantitative detection.
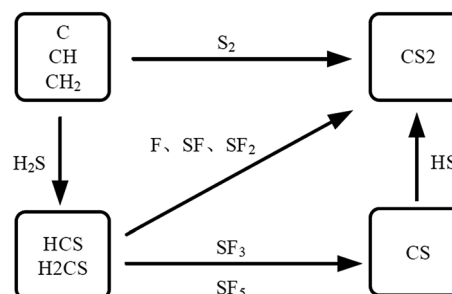
## 1    Introduction

Sulfur hexafluoride ($SF_6$) has good electrical properties and excellent arc suppression performance. As an insulating gas, $SF_6$ is widely used in a variety of high-voltage electrical equipment.[1,2] In the $SF_6$ insulation equipment, partial discharge (PD), partial overthermal faults (POF), and other failures may cause the decomposition of $SF_6$; this finding may result in $CS_2$, $SO_2$, $H_2S$, $SOF_2$, and $SO_2F_2$ decomposition components. These decomposition components on one hand will exacerbate the equipment faults, on the other hand may cause harm to the safety of personnel. Therefore, SF6 decomposition components and the monitoring of insulation faults, such as PD, must be diagnosed.[3–5]

$H_2S$ occurs mainly in the $SF_6$ overheating decomposition like PD and POF with trace moisture involved. $SF_6$ decomposes and generates $S^{2-}$ after the collision, $H_2O$ breaks and generates $H^+$. $S^{2-}$ and $H^+$ eventually combine to generate $H_2S$.[6] The chemical formula of the reaction mechanism is described as follows:

$$SF_6 + 2e \rightarrow S^{2-} + 6F \tag{1}$$

$$S^{2-} + 2H^+ \rightarrow H_2S \tag{2}$$

[a]School of Electrical Engineering, Wuhan University, Wuhan 430072, China. E-mail: xiaoxing.zhang@outlook.com

[b]State Grid Electric Power Company of Chongqing, Yongchuan, 402160, China

[c]Department of Electrical and Computer Engineering, Center for Optical Material Science and Engineering Technologies (COMSET), Clemson University, Clemson, South Carolina 29634, USA

In relevant studies, $CS_2$ occurs in PD and POF failures when the molecular structure of epoxy insulator deteriorates in relatively high temperature. Some active pieces like $CH_2$, CH and C will be generated and react with $SF_6$ or its decompositions.[7] Generate path of CS2 is showed in Fig. 1.

Among them, C atoms are derived from organic insulating materials and stainless steel, and S atoms are derived from $SF_6$. Generation of S atoms requires $SF_6$ to break six S–F bonds, which correspond to a higher energy; hence, $CS_2$ can be detected at higher temperatures. Known from the Arrhenius law[8] in the chemical reaction kinetics, the chemical reaction rate is exponentially related to the reaction temperature. When the local overheat temperature is low, the $CS_2$ generation reaction is slow; when the local overheat temperature is high, $CS_2$ generation reaction abruptly accelerates. $CS_2$ is an important characteristic component to judge the existence of solid insulation



Fig. 1    Generate path of $CS_2$.

defects. $CS_2$ detection is of great significance to the fault diagnosis of $SF_6$ insulation equipment.

At present, the detection of $SF_6$ characteristic decomposition components is achieved by two main methods: chemical detection methods and optical detection methods. Chemical gas detection methods include gas sensor method, detection tube method, and gas chromatography method;[9,10] optical methods include infrared Fourier transform spectroscopy, photoacoustic spectroscopy, and ultraviolet (UV) absorption spectroscopy. In comparison with the optical detection method, the chemical detection method has the characteristics of long detection time and high detection precision. Long detection time makes it not suitable for online monitoring. The infrared absorption spectrum can realize online monitoring. However, the infrared absorption characteristic peaks of $SF_6$ gas and various component gases are very close, and the overlapping of characteristic peaks easily occurs, which limits the detection accuracy. Photoelectric spectrum method has a high sensitivity but is susceptible to ambient temperature, pressure, and external noise.[11-13] The above methods have limitations in the online monitoring of the $SF_6$ characteristic decomposition component.

The external electrons in the molecules are excited by photons in different energy levels. The number of electron layers of different molecules and the energy levels of each layer are different; hence, difference in UV absorption spectra of different molecules is observed. One way to quantitatively study of a unknown gas can be realized by analyzing the peak position and peak of the absorption spectrum. UV differential optical absorption spectrometry (UV-DOAS), by fitting the slow absorption part of the original absorption spectrum and subtracting it, can effectively eliminate the influence of spectral absorption caused by Rayleigh scattering and Mie scattering on the gas concentration measurement and has strong anti-interference ability.[14,15]

$H_2S$ and $CS_2$, as the important decomposition products of SF6 in the PD and POF insulation failure under, have absorption peaks in the UV spectrum region. Among them, $H_2S$ absorption peaks distribute in 180–230 nm, and $CS_2$ absorption peak distribute in 190–210 nm; an overlap between the two gases' absorption peaks is found.

In 1963, Kleman *et al.* studied the absorption properties of $CS_2$ at 190–210 nm. $CS_2$ spectrum in the range of 285–340 nm was obtained by Ahmed and Kumr.[10] Due to the weak absorption at 285–340 nm band, when the light path is short or the low UV lamp power is low, the absorption cannot be measured in the band; hence, this study on the $CS_2$ UV spectral concentrated in the 190–210 nm band. In 2004, Yu *et al.* constructed a gas pool with a length of 1400 m and increased the detection limit of $CS_2$ to 2 ppb using UV absorption spectroscopy.[16] However, studies on the quantitative detection of $H_2S$ gas UV spectroscopy are few. The optical detection methods of $H_2S$ are mostly photoacoustic spectroscopy and infrared spectroscopy.[12] Studies on the quantitative determination of the two mixed gases using UV differential spectroscopy are not found.

In this paper, based on the UV differential absorption spectroscopy, the optical detection platform for $H_2S$ and $CS_2$

was constructed. First, the UV absorption spectra of the two gases were obtained according to the experiment. For each gas, the relationship between the absorption spectrum and the concentration was established by wavelet transform and frequency domain analysis. The cross-effects of the two kinds of gas absorption peaks at different concentrations were studied. The $H_2S$ concentration inversion formula in the presence of $CS_2$ was obtained. The quantitative detection method of $H_2S$ and $CS_2$ mixed gases was put forward, and the mixed gases with different mixing ratios can be detected in high accuracy. This method effectively utilizes the regularity of the absorption of two gases in the UV spectrum region, and realizes the quantitative detection of the two gases mixture, which is suitable for the quantitative detection of $SF_6$ decomposition components.

## 2 Theory

### 2.1 Principle of UV differential absorption spectrometry

One way of quantitatively detection by UV-DOAS is to utilize the absorption characteristics of gas molecules in the UV spectrum region. The measurement principle, based on Beer–Lambert law,[17] is as follows:

$$c = A(\lambda)/(\sigma(\lambda)L) \tag{3}$$

where, $c$ is the concentration of the light-absorbing medium, $A(\lambda)$ is the absorbance at the corresponding wavelength position, $\sigma(\lambda)$ is the absorption cross-section, and $L$ is the effective absorption path of the medium.

To eliminate the non-spectral noise signals, such as the dark current generated by the photodetector during the spectral acquisition process, and the background noise signal, such as the jitter of the optical fiber during the experiment, $A(\lambda)$ can be expressed as:

$$A(\lambda) = \ln\left(\frac{I'_0(\lambda) - I_N(\lambda)}{I_t(\lambda) - I_N(\lambda)}\right) \tag{4}$$

where, $I'_0(\lambda)$ is the transmitted light intensity through vessel without light-absorbing medium, $I_t(\lambda)$ is the transmitted light intensity through the light-absorbing medium, and $I_N(\lambda)$ is the dark spectrum measured when no incident light is found.

The differential absorption spectrum, as the fast-changing part, can be obtained by separating the slow-changing part from the original absorption spectrum. The fast-changing part characterizes the gas absorption spectrum information and the slow-changing part is caused by Rayleigh scattering, Mie scattering, and airflow quiver.[12] This part is defined as:

$$F(\lambda) = A(\lambda) - S(\lambda) \tag{5}$$

where,

$$S(\lambda) = \left[\sum_i c_i\sigma_{ib}(\lambda) + \varepsilon_R(\lambda) + \varepsilon_m(\lambda) + E(\lambda)\right]L \tag{6}$$

$$c' = F(\lambda)/(\sigma'(\lambda)L) \tag{7}$$

$\sigma_{ib}(\lambda)$ is the absorption cross section changing slowly with the wavelength; $\sigma'(\lambda)$ is the absorption cross section changing rapidly with the wavelength; $\varepsilon_R(\lambda)$ is the Rayleigh absorption coefficient; $E(\lambda)$ is the parameter characterizing gas jitter, instrument jitter, and other influence factors; $F(\lambda)$ is the differential absorption spectrum; and $S(\lambda)$ is the slow-changing spectrum, which can be fitted according to the basic variation of original absorbance spectrum $A(\lambda)$.

### 2.2 Absorption peaks of the two gases

The UV absorption spectrum of $H_2S$ can be obtained from the MPI-Mainz database. Fig. 2 shows the UV absorption peak data of $H_2S$.[18–23] $H_2S$ absorption peak is mainly concentrated in the range of 180–230 nm, which belongs to the deep UV region.

According to the $CS_2$ data provided by MPI-Mainz database, main absorption peaks in the UV 190–210 nm band and weak absorption peaks in the 285–340 nm band are found.[24–29] As it's shown in Fig. 3.

Therefore, due to the spectra superimposed in the wavenumber domain, $H_2S$ cannot be quantitatively analyzed by using the concentration inversion expression of single gas
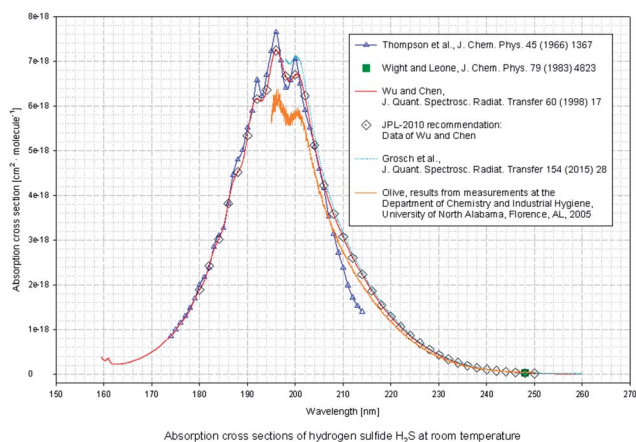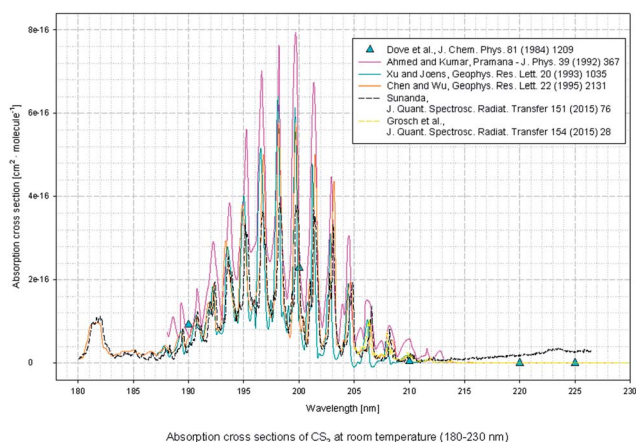
directly. However, given that $CS_2$ is not affected in the wavenumber domain by $H_2S$, $CS_2$ can be quantified by the inversion formula of $CS_2$. Therefore, if we can find the influence rule of $CS_2$ on $H_2S$, then the $H_2S$ quantification in the mixed gases can be realized. This finding is also the key to achieving simultaneous detection for mixing gas of $CS_2$ and $H_2S$.

## 3 Experiment

### 3.1 Experiment set

This platform mainly includes UV light source, gas absorption cell, spectrometer, host computer, gas sample compounder, vacuum pump, and other components, shown in Fig. 4. Among them, the UV light source (Ocean Optics D2000) can output 190–400 nm range of stable UV spectrum, a peak-to-peak stability of less than 0.005%, and per hour drift is within 0.5%. With regard the spectrometer (Ocean Optics maya2000pro spectrometer), the spectral range of 165–1100 nm, and the standard optical resolution is at 0.25 nm. Fibers (Ocean Optics QP600) can achieve 80% transmittance above 180 nm. The gas absorption cell is made of custom stainless steel. The internal light is reflected once, and the optical path length is 0.8 m. The inner wall of the cell is coated with Teflon coating, which can effectively prevent the adsorption of test gases. The gas distributor is a gas sample compounder, which has the largest dilution ratio is of $300 : 1$ and an accuracy of $\pm 1\%$ FS. Standard gases (Newradargas Co., Ltd., Wuhan) are high purity nitrogen, 2 ppm $CS_2$, and 50 ppm $H_2S$.

### 3.2 Experimental operation

We prepared different concentrations for the two kinds of single gas and the different ratios of mixed gases by gas sample compounder. The specific mix ratio is discussed in Section 3.3. The experimental gases were prepared from low to high concentration. Before the test, the gas cell was cleaned three to five times with high-purity nitrogen gas. Each time, the cell was vacuumed and inflated to atmospheric pressure with nitrogen, then left to stand for 3 min. After cleaning, the cell was inflated to atmospheric pressure with nitrogen. The dark spectrum is collected in the case of no-light, and the background spectrum
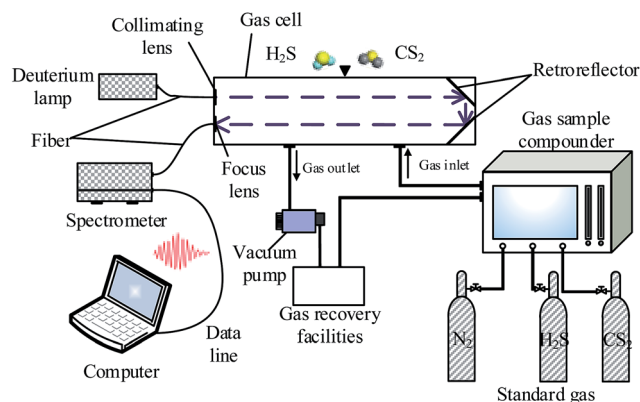


Fig. 2 UV absorption cross section spectra of $H_2S$.



Fig. 3 UV absorption cross section spectra of $CS_2$.



Fig. 4 Schematic diagram of the UV-DOAS detection system.

**Table 1** Mixture gases of $CS_2$ and $H_2S$

| CS₂ (ppb) | H₂S (ppm) | | | | |
|---|---|---|---|---|---|
| | 1 | 2 | 5 | 10 | 20 |
| 10 | | ✓ | | ✓ | |
| 20 | ✓ | | ✓ | | ✓ |
| 50 | | ✓ | | ✓ | |
| 100 | ✓ | | ✓ | | ✓ |
| 200 | | ✓ | | ✓ | |

is collected in the case of with-UV-light, and the light source is confirmed to be stable by the spectrometer before collecting the background spectrum. Finally, the test gases are collected in a low-to-high-concentration order. The gas cell was evacuated and washed twice after each detection. Each group was collected with 10 spectral data; one of which was used for quantitative analysis, and the other nine groups were used to verify the concentration inversion expression. The obtained dark spectrum, the background spectrum, and the test gas spectrum were placed into the formula (4) to calculate UV absorption spectrum. Through the baseline deduction to remove the slow-changing part of the spectrum, differential optical absorption spectrum can be obtained as described in formula (5).

### 3.3 Filters of the spectrum

The UV differential absorption spectra directly obtained by experiments cannot obtain good detection accuracy. On the one hand, the existence of some noise that cannot be removed by UV-DOAS theory. On the other hand, the measurement of mixed gases will cause the spectrum to superimpose, which is not enough to achieve the effective separation of the two gas spectra in the wavelength domain; this finding means that quantitative detection of mixing components cannot be achieved. To solve the above problems, this paper combined the wavelet transform and FFT transform to extract further the feature quantity in the

UV differential absorption spectrum and to eliminate the effect of the interference noise. In this paper, Meyer wavelet is used. The wavelet function and this wavelet's scale function are both defined in the frequency domain and have a fast convergence rate. Through the experimental test, the optimal wavelet scale for $CS_2$ and $H_2S$ filtering is 10 and 33, respectively. Interference noise in the spectrum was removed by Meyer wavelet filter, and the feature information is enhanced several times. The details are discussed in Section 4.1.

### 3.4 Gas distribution

Compared with $CS_2$, $H_2S$ are more likely to produce and with a produce higher yield in POF fault,[30,31] so go to the following concentration. For each single gas, $H_2S$ test gas was prepared in 1, 2, 5, 10, and 20 ppm, $CS_2$ test gas were prepared in 10, 20, 50, 100 and 200 ppb. The mixtures of both gases prepared in nitrogen because $SF_6$ and $N_2$ neither has absorption in 190–400 nm and don't have a interference for detection.

The mixing gas for the two gases is shown in Table 1, where, "✓" indicates that the combination is prepared.

The gas distribution process can be described as follows: (a) $CS_2$ was kept constant at 20 or 100 ppb, and we adjusted the $H_2S$ at 1, 5, and 20 ppm from low to high concentration at each $CS_2$ concentration. (b) $H_2S$ was kept at 2 or 10 ppm unchanged, adjusting the $CS_2$ at 10, 50, and 200 ppb in turn from low to high concentrations at each $H_2S$ concentration.

## 4 Results and discussion

### 4.1 Single-gas inversion expression

**4.1.1 $H_2S$.** Through a large number of experiments, the results are shown in Fig. 5. Fig. 5(a) shows the UV absorption spectra of $H_2S$ at different concentrations. The overall absorbance increases with the increase of the concentration. UV absorption of $H_2S$ ranges from 190 nm to 250 nm; however, the narrow band absorption is only around 190–210 nm.
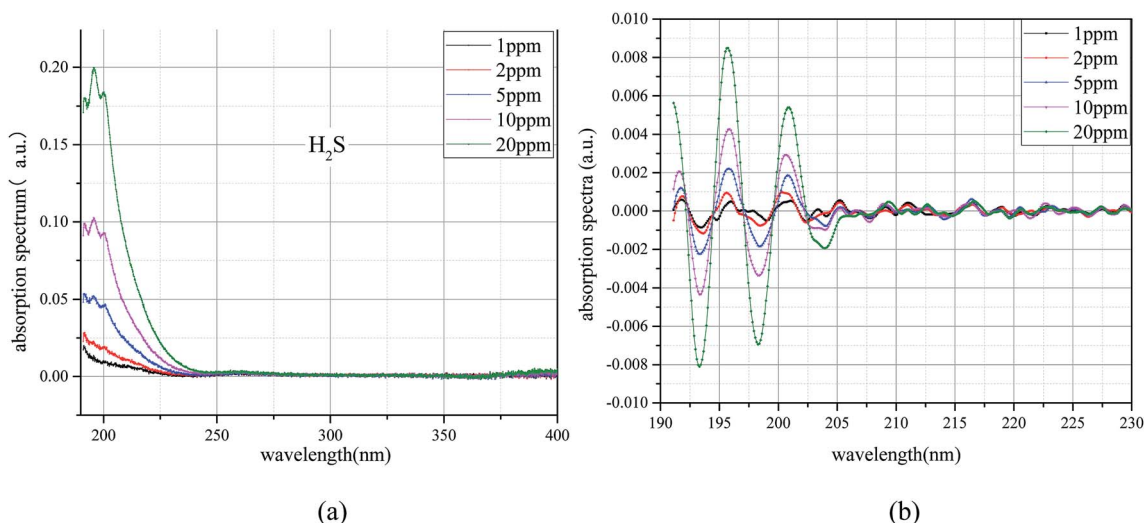


(a)



(b)

**Fig. 5** UV spectrum of $H_2S$. (a) UV absorption spectrum. (b) Differential spectrum.

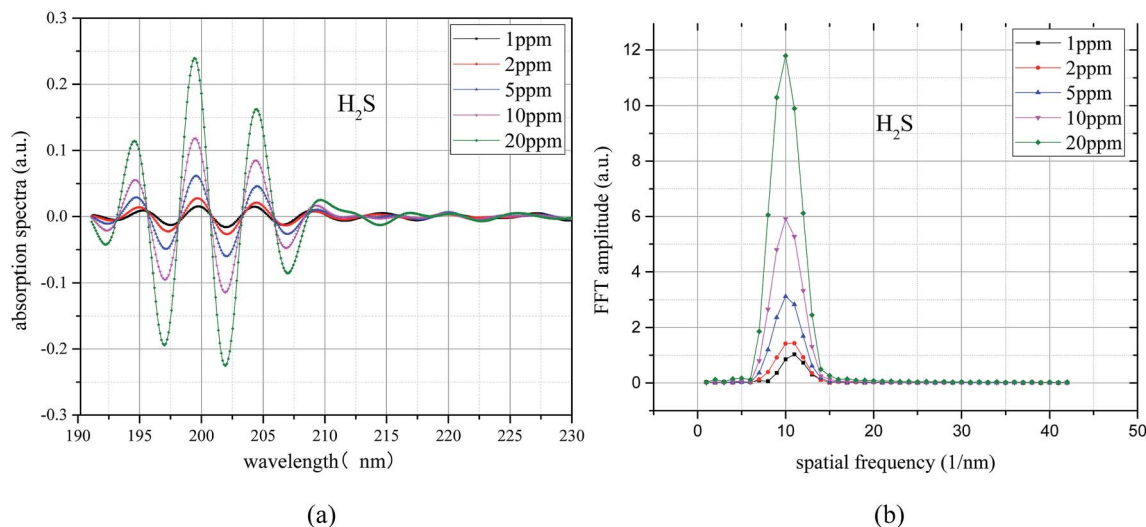**Fig. 6** H$_2$S differential absorption spectroscopy after filtering and its FFT spectrum. (a) Differential spectrum after filter. (b) FFT frequency spectrogram.

Concentration of H$_2$S of 5, 10, and 20 ppm showed a narrow band absorption, whereas the narrow band absorption is very weak for 2 and 1 ppm H$_2$S. Fig. 5(b) is the corresponding UV difference absorption spectra extracted from the UV absorption spectra of H$_2$S at different concentrations. Data are not found with regard the absorption in the rear band of 210 nm, and the H$_2$S at each concentration shows narrowband absorption. The narrowband absorption of H$_2$S gradually increases with the increase of the concentration. The UV differential absorption spectra of H$_2$S are affected by the high-frequency noise; the lower the concentration, the more serious the influence there is.

A bandpass filter algorithm for the extraction of UV differential absorption spectra of H$_2$S was constructed by using Meyer wavelet. The differential absorption spectrum after treatment is shown in Fig. 6(a), and the UV absorption spectrum after filtering is further transformed by FFT; the results shown in Fig. 6(b). Fig. 6(a) shows that (1) the characteristic information of the UV differential absorption spectrum is very concentrated, almost no high and low wave number of noise interference, (2) peaks of different concentrations appear at the same position (10 nm$^{-1}$), and the peak value of H$_2$S increases with the increase of H$_2$S concentration; this finding means that the concentration can be well characterized.

To avoid the randomness of single data point, the algebraic sum of the FFT values of three points (9 nm$^{-1}$, 10, and 11 nm$^{-1}$) is chosen as the FFT eigenvalues to characterize the trace H$_2$S concentration. The FFT eigenvalues at different concentrations were calculated. Least squares method was used to linearly fit the H$_2$S concentration and its corresponding FFT eigenvalues. The fitting results are shown in Fig. 7. The FFT eigenvalues and H$_2$S concentration have a high degree of linearity, which reaches 0.9999 ($R^2$). H$_2$S concentration can be obtained by inversion expression as:

$$y = 1.564x + 0.571 \qquad (8)$$

where, $y$ is the FFT eigenvalue of the H$_2$S, and $x$ is the H$_2$S concentration (ppm). The uncertainty of slope and intercept is $4.83 \times 10^{-3}$ and $4.98 \times 10^{-2}$.

**4.1.2 CS$_2$.** The obtained CS$_2$ UV absorption spectrum at each concentration is shown in Fig. 8(a). CS$_2$ has UV absorption at each concentration, and the absorption is increased with the increase of concentration. The interval between the narrow band absorption peaks is significantly smaller than that of H$_2$S. The UV differential absorption spectra at each concentration were extracted, and the results are shown in Fig. 8(b). The UV differential absorption spectra of CS$_2$ at different concentrations show similar characteristics. With the increase of the concentration, the differential absorption is enhanced. When
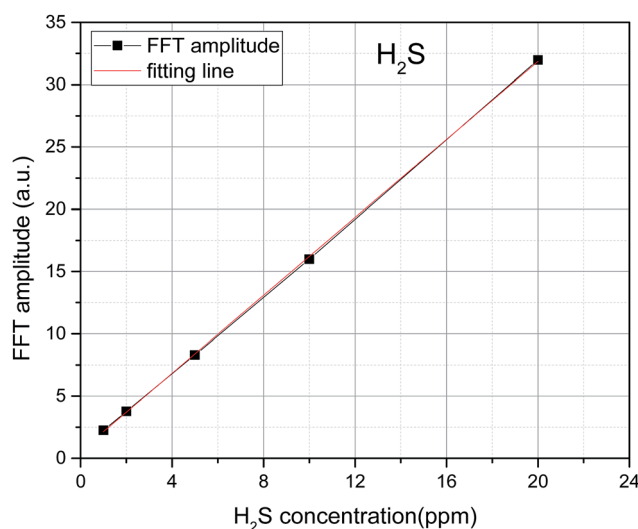


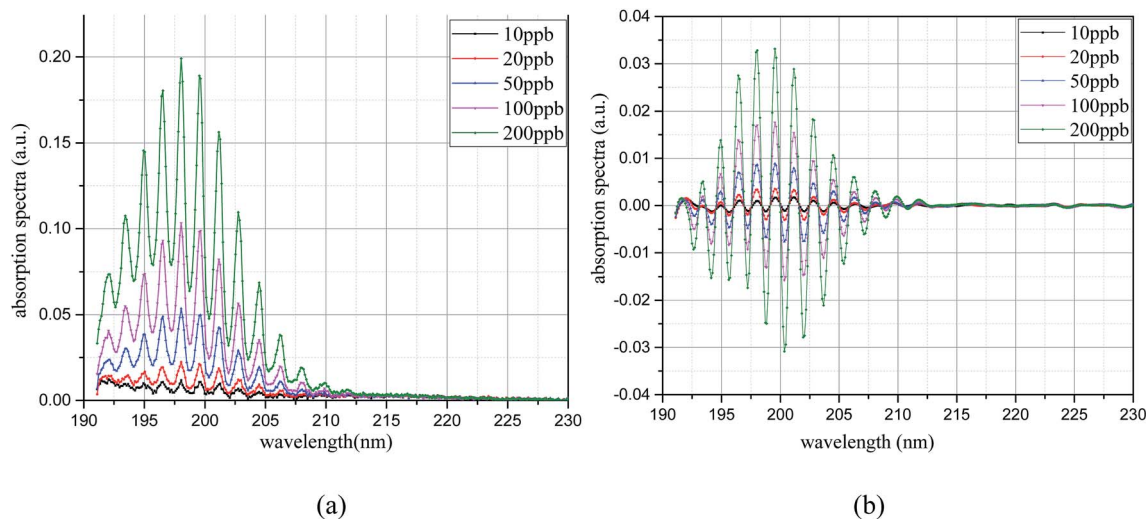**Fig. 7** Relationship between FFT eigenvalue and H$_2$S concentration.

**Fig. 8** UV spectrum of $CS_2$. (a) UV absorption spectrum. (b) Differential spectrum.

the $CS_2$ concentration is low, high-frequency noise in the differential spectrum is observed, and the spectrum is easily affected.

The UV differential absorption spectra of each $CS_2$ concentration were filtered using the Meyer wavelet; the results are shown in Fig. 9(a). In the figure, the differential absorption spectra of each concentration after filtering treatment are more obvious and the spectrum is very smooth. Almost no interference information is found. With the increase of concentration, the spectral characteristics of $CS_2$ are similar, and the absorption gradually strengthens. The FFT frequency spectrogram results are shown in Fig. 9(b). Fig. 9(b) shows that the characteristic information is concentrated after filtering treatment, and the peak appears at 30 nm$^{-1}$, which is different from $H_2S$. With the increase of $CS_2$ concentration, the FFT value increases simultaneously. Therefore, the UV differential absorption spectrum after filtering and its FFT value in the wavenumber

domain have the ability to realize quantitative analysis of $CS_2$. The FFT eigenvalues of the UV absorption spectrum were used for $CS_2$ concentration inversion.

The algebraic sum of the FFT values (9, 30, and 31 nm$^{-1}$) is chosen as the FFT eigenvalues to characterize the concentration of $CS_2$, and the least squares method is used to linearly fit the concentration and FFT eigenvalues. In Fig. 10, results show a high degree of linear relationship between the FFT eigenvalues and $CS_2$ concentration, and the linearity ($R^2$) is as high as 0.9998. The inversion expression is:

$$y = 0.1434x + 0.1062 \qquad (9)$$

where, $y$ represents the FFT eigenvalue of the $CS_2$, and $x$ represents the $CS_2$ concentration in ppb. The uncertainty of slope and intercept is $7.58 \times 10^{-4}$ and $7.76 \times 10^{-2}$.
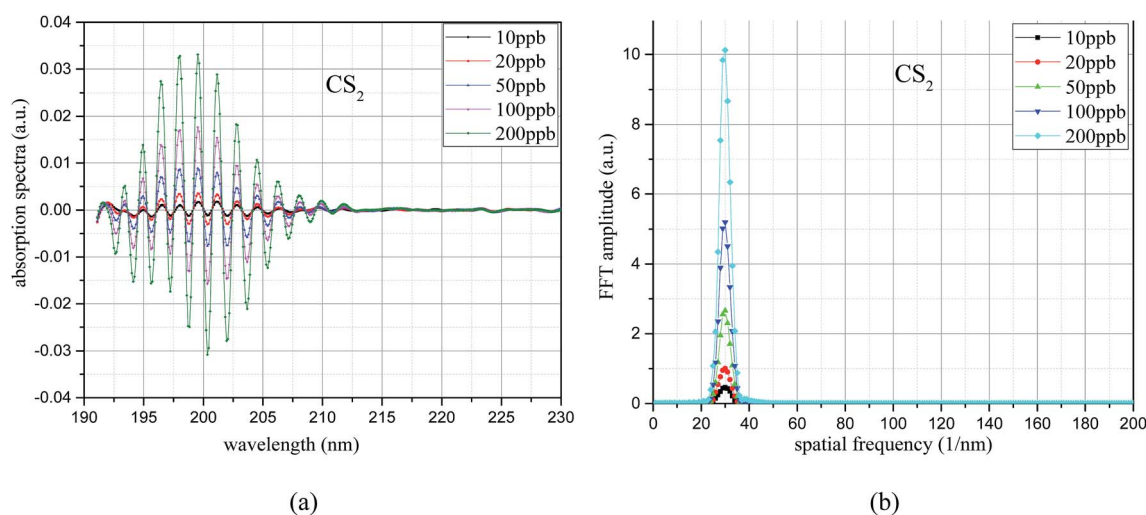


**Fig. 9** UV difference absorption spectroscopy after filtering and its FFT spectrum. (a) Differential spectrum after filter. (b) FFT frequency spectrogram.
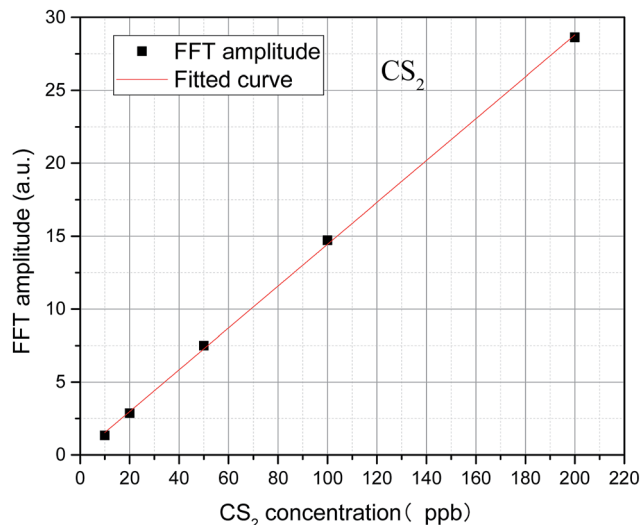
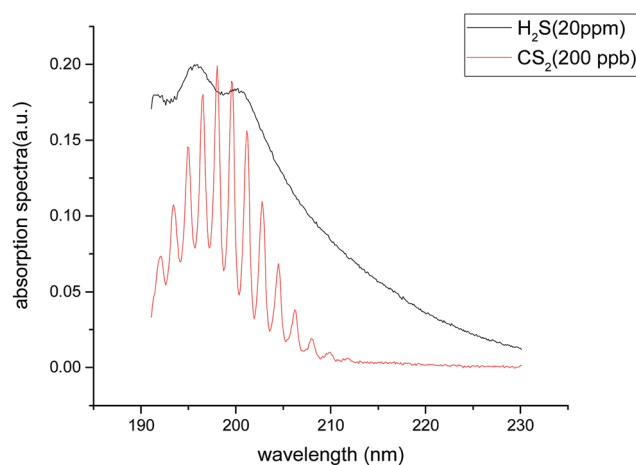Fig. 10 Relationship between FFT eigenvalue and $CS_2$ concentration.



Fig. 11 The superposition of the two respectively UV absorption spectra of two gases.

### 4.2 Mixed gas detection

In Fig. 1 and 2, the absorption coefficient of $CS_2$ is about two orders of magnitude larger than that of $H_2S$. To visually show the intersection of the two kinds of gases near UV 200 nm band, the spectra of 20 part per million (ppm) of $H_2S$ and 200 part per billion (ppb) of $CS_2$ are detected, and the two are superimposed on Fig. 3.

In Fig. 11, the two gases in the UV spectrum region have a serious cross; this finding means that each absorption spectra of the two gases cannot be separated directly by UV differential spectroscopy, and the two gas concentrations cannot be obtained by inversion method. The slow-changing part of the absorption spectrum was removed by baseline deduction, and the differential absorption spectrum was obtained. The obtained differential spectrum was inverted into the frequency domain by FFT transform. The results are shown in Fig. 12.

Fig. 12 shows that the differential absorption spectra of the two gases are superimposed in the wavelength domain, and the UV differential absorption spectra of $H_2S$ are all submerged in the spectra of $CS_2$. Fig. 4(b) shows that the eigenvalues of $CS_2$ in wavenumber domain are not affected by $H_2S$; however, the $CS_2$ contains characteristic information for $H_2S$ quantification, which will have an effect on the quantitative detection of $H_2S$.

**4.2.1 Inversion results.** The mixed gases are prepared as discussed in Section 3.4. The spectral data of each mixture were collected in 10 groups to avoid experimental errors. The differential absorption spectra of the two gases were extracted by the filters, and the $CS_2$ and $H_2S$ concentrations were calculated by using the concentration inversion expressions in Section 4.1. The results are shown in Table 2. The concentrations were calculated by taking the average after the minimum and maximum were removed in 1 of the 10 groups. $\Delta_h$ is the difference value between the calculation results and the actual concentration of $H_2S$. $\delta$ is the percentage of error. In Table 2, the relationship between the inversion concentration and the actual concentration of the two gases were described.

In Fig. 13, the linearity ($R^2$) of $CS_2$ concentration is up to 0.9997 mixed with different $H_2S$ concentrations; this result indicates that the presence of mixed $H_2S$ has little effect on $CS_2$ concentration inversion. In Table 2 and Fig. 14, when the $CS_2$
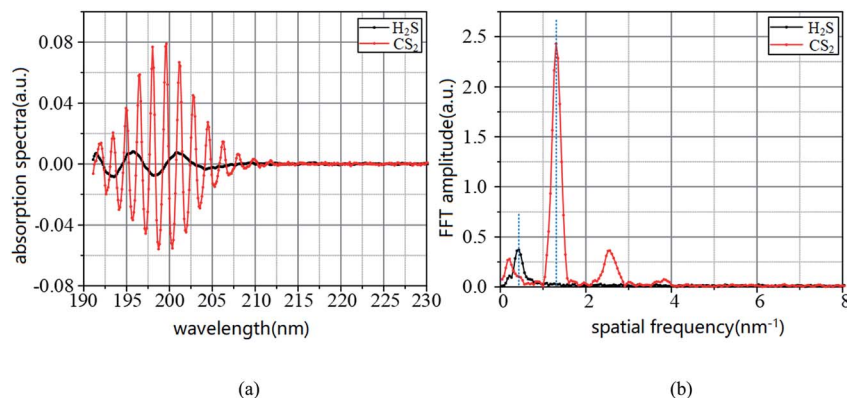


(a)

(b)

Fig. 12 UV difference absorption spectra of $CS_2$ and $H_2S$ and its FFT spectra. (a) Differential spectrum. (b) FFT frequency spectrogram.

**Table 2** Direct inversion results of $CS_2$ and $H_2S$ mixed gases

| $CS_2$ (ppb) | | Inversion concentration | | | $\Delta_h$ (ppm) | $\delta$ (%) |
|---|---|---|---|---|---|---|
| 20 | | 19.7 | 19.9 | 19.0 | | |
| $H_2S$ (ppm) | 1 | 0.96 | | | −0.04 | 4 |
| | 5 | 4.95 | | | −0.05 | 1 |
| | 20 | 20.19 | | | 0.19 | 0.95 |

| $CS_2$ (ppb) | | Inversion concentration | | | $\Delta_h$ (ppm) | $\Delta$ (%) |
|---|---|---|---|---|---|---|
| 100 | | 99.8 | 101.3 | 99.01 | | |
| $H_2S$ (ppm) | 1 | 3.03 | | | 2.03 | 203 |
| | 5 | 6.91 | | | 1.91 | 38.2 |
| | 20 | 21.85 | | | 1.85 | 9.25 |

| $H_2S$ (ppm) | | Inversion concentration | | | $\Delta_h$ (ppb) | $\delta$ (%) |
|---|---|---|---|---|---|---|
| 2 | | 1.99 | 2.58 | 6.57 | | |
| $CS_2$ (ppb) | 10 | 8.9 | | | −0.01 | 0.1 |
| | 50 | 51.4 | | | 0.58 | 1.16 |
| | 200 | 196.5 | | | 4.57 | 2.23 |

| $H_2S$ (ppm) | | Inversion concentration | | | $\Delta_h$ (ppb) | $\Delta$ (%) |
|---|---|---|---|---|---|---|
| 10 | | 10.23 | 10.56 | 14.10 | | |
| $CS_2$ (ppb) | 10 | 9.5 | | | 0.23 | 2.3 |
| | 50 | 51.4 | | | 0.56 | 1.12 |
| | 200 | 197.1 | | | 4.10 | 2.05 |

concentration is small (10 and 20 ppb), little effect on the inversion of $H_2S$ is observed. However, when the concentration of $CS_2$ is large (50, 100, and 200 ppb), the inversion of $H_2S$ concentration is disturbed. Besides, the effect basically shows a linear increase with the increase of $CS_2$ concentration. The two fitting lines shown in Fig. 14 are almost parallel; this result indicates that the same concentration of $CS_2$ has a relatively close effect on different concentrations of $H_2S$. Thus, the lower concentration of $H_2S$ is disturbed more by $CS_2$.

**4.2.2 Correction expression of $H_2S$.** In accordance to the previous section, the concentration of $CS_2$ in the mixed gases of $H_2S$ and $CS_2$ can be calculated directly, and the $H_2S$ concentration inversion expression must be corrected. Considering the $H_2S$ detection limit, and the unavoidable errors, such as gas operation. Low concentration detection should be of priority. The concentration effects were calculated through the three concentrations. $CS_2$ in 50, 100, and 200 ppb were set to 0.6, 2.0, and 4.6 ppm $H_2S$ increase. The correction expression was
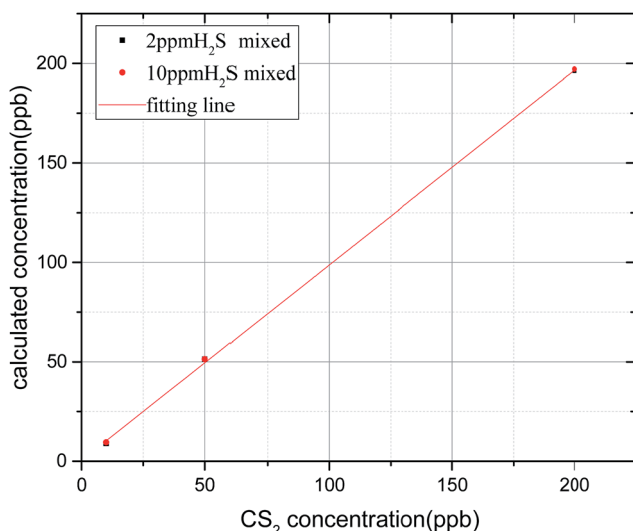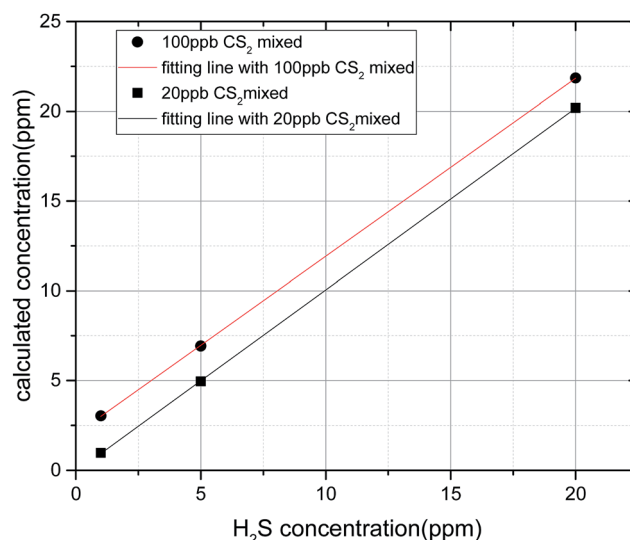


**Fig. 13** Inversion concentration of $CS_2$ with different concentrations of $H_2S$.



**Fig. 14** Inversion concentration of $H_2S$ with different concentrations of $CS_2$.

**Table 3**  Revised inversion results of $H_2S$ in mixed gases

| (a) | | | (b) | | | (c) | | |
|---|---|---|---|---|---|---|---|---|
| 20 ppb $CS_2$ | | | 50 ppb $CS_2$ | | | 150 ppb $CS_2$ | | |
| $c_H$ | $c_h$ | $\Delta_h$ | $c_H$ | $c_h$ | $\Delta_h$ | $c_H$ | $c_h$ | $\Delta_h$ |
| 1 | 0.65 | −0.35 | 1 | 0.97 | 0.03 | 1 | 1.12 | 0.12 |
| 2 | 1.82 | 0.18 | 2 | 1.99 | 0.01 | 2 | 1.67 | −0.33 |
| 5 | 5.04 | 0.04 | 5 | 5.15 | 0.15 | 5 | 4.50 | 0.50 |
| 10 | 10.29 | 0.29 | 10 | 10.27 | 0.27 | 10 | 10.03 | 0.03 |
| 15 | 15.27 | 0.27 | 15 | 15.20 | 0.20 | 15 | 14.85 | −0.15 |
| 20 | 20.27 | 0.27 | 20 | 19.80 | −0.2 | 20 | 19.81 | −0.19 |

determined based on the determined influence value, shown as formula (10).

$$\Delta_h = 0.0259 \times c_c - 0.45 \ (R^2 = 0.9997) \tag{10}$$

where, $\Delta_h$ represents the increase in $H_2S$ caused by $CS_2$ (unit: ppm). $c_c$ represents the concentration of $CS_2$ (unit: ppb).

**4.2.3 Inversion with correction expression.** We changed a set of gas concentration to check the correction expression. The concentration of $H_2S$ in mixed gases was detected and calculated again; results are shown in Table 3 $c_H$ is the actual concentration of $H_2S$. $c_h$ is the inversion result. $\Delta_h$ is the difference value between $c_H$ and $c_h$, in ppm. The results show the effect of the correction expression, and the inversion values can nearly reflect the actual concentration.

In Fig. 15, the corrected straight line has a high linearity, and the concentration inversion of $H_2S$ is very accurate. The linearity ($R^2$) is 0.9994, which means that the correction expression can be used in the detection of the two gas mixture.

Therefore, for the quantitative detection of $H_2S$ and $CS_2$ mixed gases, the concentration of $H_2S$ and $CS_2$ can be calculated by the expressions (8) and (9) after the differential spectrum was obtained. Then, $H_2S$ was corrected with expression (10) to obtain accurate concentration.
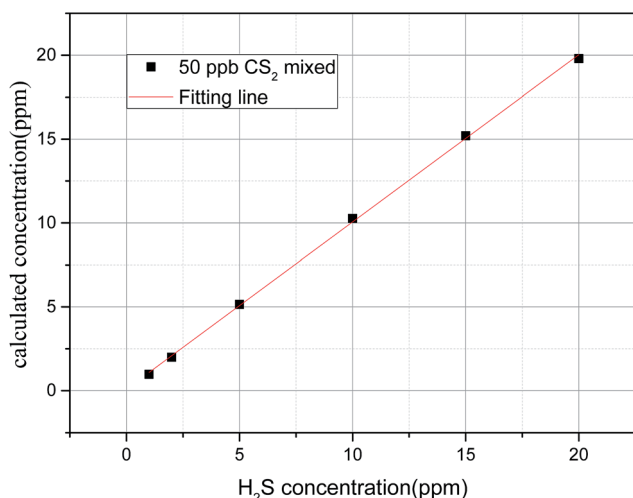


**Fig. 15**  Fitting straight line of $H_2S$ after correction.

## 5  Conclusion

In this paper, the detection platform of $H_2S$ and $CS_2$ based on UV absorption spectroscopy was established. First, two kinds of single gases were detected, and the concentration inversion expressions of the two gases were obtained. After that, the mixed gases at different ratios were detected. $H_2S$ has little effect on the detection of $CS_2$, and the effect of $CS_2$ on $H_2S$ concentration inversion is linear with $CS_2$ concentration. Basing on the data analysis, we obtained the correction expression of $CS_2$ gas to $H_2S$ concentration. Expression validity was proved by the actual data verification. Hence, the $H_2S$ and $CS_2$ gas can be detected by using the proposed modified detection expressions, which can realize the high-precision quantitative detection of the two gases and provide technical support for the online monitoring of $SF_6$ decomposition components.

## Conflicts of interest

There are no conflicts to declare.

## References

1  L. G. Christophorou and J. K. Olthoff, Electron Interactions with SF6, *IEEE International Conference on Plasma Science, 1996. IEEE Conference Record*, IEEE, 1999, p. 107.

2  F. Y. Chu, SF6 Decomposition in Gas-Insulated Equipment, *IEEE Trans. Electr. Insul.*, 1986, **EI-21**(5), 693–725.

3  J. Tang, F. Zeng, J. Pan, *et al.*, Correlation analysis between formation process of SF6, decomposed components and partial discharge qualities, *IEEE Trans. Dielectr. Electr. Insul.*, 2013, **20**(3), 864–875.

4  X. Zhang, J. Zhang, Y. Jia, *et al.*, TiO2 Nanotube Array Sensor for Detecting the SF6 Decomposition Product SO2, *Sensors*, 2012, **12**(3), 3302–3313.

5  S. Pokharel, Spatial analysis of rural energy system, *Int. J. Geogr. Inform. Sci.*, 2000, **14**(8), 855–873.

6  F. Zeng, J. Tang, Y. Xie, *et al.*, Experiment Study of Trace Water and Oxygen Impact on SF6 Decomposition Characteristics Under Partial Discharge, *Journal of Electrical Engineering & Technology*, 2015, **10**(4), 1787–1796.

7  X. Zhang, H. Zhou, C. Chen, *et al.*, Ultraviolet Differential Optical Absorption Spectrometry: Quantitative Analysis of the CS2 Produced by SF6 Decomposition, *Meas. Sci. Technol.*, 2017, **28**, 115102.

8  M. Mortimer and P. G. Taylor, *Chemical kinetics and reaction mechanism*, Springer Verlag, Berlin, Germany, 2002.

9  X. Zhang, L. Yu, Y. Gui, *et al.*, First-principles study of SF6, decomposed gas adsorbed on Au-decorated graphene, *Appl. Surf. Sci.*, 2016, **367**, 259–269.

10  F. Y. Chu, SF6 decomposition in gas-insulated equipment, *IEEE Trans. Electr. Insul.*, 1986, (5), 693–725.

11  X. Zhang, H. Liu, J. Ren, *et al.*, Fourier transform infrared spectroscopy quantitative analysis of SF 6 partial discharge decomposition components, *Spectrochim. Acta, Part A*, 2015, **136**, 884–889.

12 X. Zhang, Z. Cheng and X. Li, Cantilever Enhanced Photoacoustic Spectrometry: Quantitative Analysis of the Trace H2S produced by SF6 Decomposition, *Infrared Phys. Technol.*, 2016, **78**, 31–39.

13 X. Cui, C. Lengignon, W. Tao, *et al.*, Photonic sensing of the atmosphere by absorption spectroscopy, *J. Quant. Spectrosc. Radiat. Transfer*, 2012, **113**(11), 1300–1316.

14 M. Wenig, B. Jähne and U. Platt, Operator representation as a new differential optical absorption spectroscopy formalism, *Appl. Opt.*, 2005, **44**(16), 3246–3253.

15 J. Mellqvist and A. Rosén, DOAS for flue gas monitoring—I. Temperature effects in the UV/visible absorption spectra of NO, NO2, SO2 and NH3, *J. Quant. Spectrosc. Radiat. Transfer*, 1996, **56**(2), 187–208.

16 Y. Yu, A. Geyer, P. Xie, B. Galle, L. Chen and U. Platt, Observations of carbon disulfide by differential optical absorption spectroscopy in Shanghai, *Geophys. Res. Lett.*, 2004, **31**, L11107.

17 L. Wang, Y. Zhang, X. Zhou, *et al.*, Optical sulfur dioxide sensor based on broadband absorption spectroscopy in the wavelength range of 198–222 nm, *Sens. Actuators, B*, 2017, **241**, 146–150.

18 S. D. Thompson, D. G. Carroll, F. Watson, *et al.*, Electronic Spectra and Structure of Sulfur Compounds, *J. Chem. Phys.*, 1966, **45**(5), 1367–1379.

19 C. A. Wight and S. R. Leone, Vibrational state distributions and absolute excitation efficiencies for T-V transfer collisions of NO and CO with H atoms produced by excimer laser photolysis, *J. Chem. Phys.*, 1983, **79**(10), 4823–4829.

20 C. Y. R. Wu and F. Z. Chen, Temperature-dependent photoabsorption cross sections of H2S in the 1600–2600 Å region, *J. Quant. Spectrosc. Radiat. Transfer*, 1999, **61**(2), 265–271.

21 L. Chen, J. Wu and R. Jia, *et al.*, Recommendation on Uncertain Services, *IEEE International Conference on Web Services*, IEEE Computer Society, 2010, pp. 683–684.

22 H. Grosch, A. Fateev and S. Clausen, UV absorption cross-sections of selected sulfur-containing compounds at temperatures up to 500 °C, *J. Quant. Spectrosc. Radiat. Transfer*, 2015, **154**, 28–34.

23 B. Olive, *Result from measurements at the department of chemistry and industrial hygiene*, University of North Alabama, Florence, al, 2005.

24 J. E. Dove, H. Hippler, H. J. Plach, *et al.*, Ultraviolet spectra of vibrationally highly excited CS2 molecules, *J. Chem. Phys.*, 1984, **81**(3), 1209–1214.

25 S. M. Ahmed and V. Kumar, Measurement of photoabsorption and fluorescence cross-sections for CS 2, at 188.2–213 and 287.5–339.5 nm, *Pramana*, 1992, **39**(4), 367–380.

26 H. Xu and J. A. Joens, CS2 absorption cross-section measurements from 187 nm to 230 nm, *Geophys. Res. Lett.*, 1993, **20**(11), 1035–1037.

27 F. Z. Chen and C. Y. R. Wu, High, room and low temperature photoabsorption cross sections of CS2 in the 1800–2300 Å region, *Geophys. Res. Lett.*, 1995, **22**(16), 2131–2134.

28 S. K. Kumar, A. Shastri, A. K. Das and B. N. Raja Sekhar, Electronic states of carbon disulphide in the 5.5–11.8 eV region by VUV photo absorption spectroscopy, *J. Quant. Spectrosc. Radiat. Transfer*, 2015, **151**, 76–87.

29 H. Grosch, A. Fateev and S. Clausen, UV absorption cross-sections of selected sulfur-containing compounds at temperatures up to 500 °C, *J. Quant. Spectrosc. Radiat. Transfer*, 2015, **154**, 28–34.

30 L. Cheng, J. Tang and X. Huang, *et al.*, SF6 partial overheating decomposition characteristics with organic insulating materials, *Gaodianya Jishu/high Voltage Engineering*, 2015, vol. 41(2), pp. 453–460.

31 F. Zeng, *et al.*, Decomposition characteristics of SF6 under thermal fault for temperatures below 400 °C, *IEEE Trans. Dielectr. Electr. Insul.*, 2014, **21**(3), 995–1004.